Outlier galaxy images in the Dark Energy Survey and their identification with unsupervised machine learning

Lior Shamir

Department of Computer Science, Kansas State University
1701 Platt St
Manhattan, KS 66506, USA

Abstract

The Dark Energy Survey is able to collect image data of an extremely large number of extragalactic objects, and it can be reasonably assumed that many unusual objects of high scientific interest are hidden inside these data. Due to the extreme size of DES data, identifying these objects among many millions of other celestial objects is a challenging task. The problem of outlier detection is further magnified by the presence of noisy or saturated images. When the number of tested objects is extremely high, even a small rate of noise or false positives leads to a very large number of false detections, making an automatic system impractical. This study applies an automatic method for automatic detection of outlier objects in the first data release of the Dark Energy Survey. By using machine learning-based outlier detection, the algorithm is able to identify objects that are visually different from the majority of the other objects in the database. An important feature of the algorithm is that it allows to control the false-positive rate, and therefore can be used for practical outlier detection. The algorithm does not provide perfect accuracy in the detection of outlier objects, but it reduces the data substantially to allow practical outlier detection. For instance, the selection of the top 250 objects after applying the algorithm to more than $2 \cdot 10^6$ DES images provides a collection of uncommon galaxies. Such collection would have been extremely time-consuming to compile by using manual inspection of the data.

1. Introduction

The deployment of digital sky surveys driven by powerful robotic telescopes has enabled the collection of very large astronomical databases. Surveys such as Sloan Digital Sky Survey (SDSS), the Panoramic Survey Telescope and Rapid Response System (Pan-STARRS) the and the Dark Energy Survey (DES) are some of the world's most productive scientific instruments, generating databases of billions of astronomical objects. While these databases are far too large to be inspected manually, future Earth-based and space-based instruments are expected to generate even larger databases, further stressing the ability to analyze the data. Space-based instruments such as Euclid, Roman, and the Chinese Survey Space Telescope (CSST), as well as ground-based telescopes such as the Vera Rubin Observatory are expected to transform the field of astronomy by the generation of unprecedented amounts of astronomical data.

While most celestial objects in these databases can be assumed to be of known types, it is likely that these databases also contain rare objects of paramount scientific interest. The distinction between a "peculiar" and a "non-peculiar" galaxy is difficult and subjective to formalize (Nairn and Lahav, 1997). It is determined by its complex visual appearance and degree of similarity to known galaxy types.

Galaxies that cannot be associated with a stage in a known morphological classification scheme such as the Hubble Sequence can provide unique information about the history of the Universe and galaxy evolution (Gillman et al., 2020), and therefore identifying and studying of these galaxies can be of scientific value (Bettoni et al., 2001; Casasola et al., 2004; Abraham and van den Bergh, 2001). Known types of peculiar galaxies are ring galaxies, which can form into a ring shape due to collisions (Appleton and Struck-Marcell, 1996) or instability of the galaxy bars (Sellwood and Moore, 1999). Another common type of peculiar galaxies are tidally distorted galaxies, with unusual shapes formed due to the gravity field of another galaxy, leading to tidal tails or other unusual morphological features. Irregular galaxies (Gallagher and Hunter, 1984) do not have defined expected shapes, and can contain higher amounts of gas and dust. Gravitational lenses can cause regular galaxies to appear distorted to an Earth-based observer, and while these galaxies are not peculiar they can be identified in digital sky surveys by their unusual shape. Dust lanes can also make galaxies seem unusual due to the reduction of light blocked by the dust lane (Möllenhoff and Bender, 1989; Athanassoula, 1992). Other types of peculiar galaxies include older forms such as quasar and blazars. Peculiar galaxies are of scientific importance, as they can carry substantial information about the past, present, and future Universe. For instance, strong gravitational lenses were used to determine the Hubble constant with high accuracy (Suyu et al., 2017; Wong et al., 2020). Statistical analysis of galaxy merger history can also be used to test the validity of cosmological models (Conselice et al., 2014; Conselice, 2014).

An example of a collection of peculiar galaxies is the Atlas of Peculiar Galaxies (Arp, 1966; Arp and Madore, 1975).

While that catalog was useful for studying peculiar galaxies, it required over a decade to prepare. Other catalogs include collections of peculiar galaxies of a certain defined type such as the collection of collisional ring galaxies (Madore et al., 2009). Manual observation of a large number of galaxies can lead to identification of peculiar galaxies, as was demonstrated by Nair and Abraham (2010), who annotated a large number of galaxies and identified several peculiar galaxies through that process. Kaviraj (2010) identified 70 peculiar systems in stripe 82 of SDSS. Manual analysis also led to the identification of irregular and interacting galaxies imaged by the Vatican Advanced Technology Telescope (Taylor et al., 2005).

Manual analysis is limited in its throughput, and therefore does not allow to analyze the extremely large databases collected by modern digital sky surveys. For instance, the Vera Rubin Observatory is expected to collect image data of more than 10^{10} galaxies. Even if each galaxy can be analyzed manually in 10 seconds, analyzing the entire database will take over 3000 years of human labor. One proposed solution for increasing the throughout was to use crowdsourcing of non-expert volunteers. An example of an unusual objects identified in that manner is "Hanny's Voorwerp" (Lintott et al., 2009), as well as a large number of ring galaxies (Finkelman et al., 2012; Buta, 2017).

As digital sky surveys become increasingly more powerful, manual identification becomes impractical. General methods to automate the analysis of galaxy images include model-driven methods such as GIM2D (Simard, 1999), GALFIT (Peng et al., 2002), CAS (Conselice, 2003), Gini (Abraham et al., 2003), Ganalyzer (Shamir, 2011), and SpArcFiRe (Davis and Hayes, 2014). Other methods are based on machine learning (Shamir, 2009; Huertas-Company et al., 2009; Banerji et al., 2010; Kuminski et al., 2014; Dieleman et al., 2015; Graham, 2019; Mittal et al., 2019; Hosny et al., 2020; Cecotti, 2020; Cheng et al., 2020). For instance, Huertas-Company et al. (2009) used Support Vector Machines (SVM) to classify galaxies by their broad morphological type. Banerji et al. (2010) demonstrated as early implementation of an artificial neural network to distinguish between elliptical and spiral galaxies. Dieleman et al. (2015) applied deep neural networks to estimate the expected manual annotations of certain morphological features of galaxies. More modern approaches are based on convolutional neural networks (Hosny et al., 2020; Cecotti, 2020; Cheng et al., 2020). The application of these methods to image data collected by digital sky surveys also led to catalogs (Huertas-Company et al., 2015a,b; Shamir and Wallin, 2014; Kuminski and Shamir, 2016; Goddard and Shamir, 2020). Machine learning algorithms were also used to identify unusual galaxies, such as galaxy mergers (Margalef-Bentabol et al., 2020), and peculiar galaxy mergers (Shamir and Wallin, 2014).

Determinstic model-driven approaches can be developed and adjusted to detect specific defined types of galaxies such as ring galaxies (Timmis and Shamir, 2017; Shamir, 2020) and gravitational lenses (Jacobs et al., 2019b; Liu et al., 2021; Wilde et al., 2022). Methods for automatic detection of strong lenses in large databases generated by ground-based sly surveys such as DES (Jacobs et al., 2019b), KiDS (Petrillo et al., 2019), HSC (Wong et al., 2022), and DECal (Huang et al., 2020). These algorithms normally cannot match the same level of completeness as manual analysis, but their ability to scan much larger datasets allows them to identify more objects than manual detection (Shamir, 2020). Such algorithms are designed for specific and previously known morphological types, and therefore cannot identify objects of types that were not known when the algorithm was designed. That can be done by using unsupervised machine learning, where the algorithm learns automatically from the data, and can identify objects that are different from the "typical" objects in the database. This paper describes the application of a method based on machine learning to image data acquired by the Dark Energy Survey (DES). The process leads to a collection of galaxies identified as the most different from the other "typical" galaxies as determined by the algorithm.

2. Data

The image data used in this study is data from the Dark Energy Survey (Perez et al., 2018; Morganson et al., 2018; Flaugher et al., 2015) Data Release 1 (Perez et al., 2018). The Dark Energy Survey (DES) uses the Dark Energy Camera (DECam) of the four-meter Blanco Telescope (Diehl et al., 2012). It covers a footprint of around $5 \cdot 10^3 deg^2$ (Abbott et al., 2018) in the Southern hemisphere. The primary goal of DES is the studying of dark energy, but it can also be used as a general-purpose powerful digital sky survey (Abbott et al., 2016).

To select objects that are galaxies, the initial list of objects included objects identified as de Vaucouleurs $r^{1/4}$ profiles, exponential disks, or round exponential galaxies. To avoid faint objects, only objects brighter than 20.5 magnitude in one or more of the g, r or z bands were included. In DES DR1, $\sim 1.9 \cdot 10^8$ objects met that criteria. Due to the time required to download and analyze a dataset of the size, $\sim$10% of the data was used in this experiment, leading to a dataset of $2 \cdot 10^6$ objects. The images were downloaded using the *cutout* API of the DESI Legacy Survey, and the downloading was complete after 32 days of continuous data retrieval. The image are in the JPEG image format and dimensionality of 256×256. The JPEG format does not allow accurate photometric measurements, but it allows to combine information from the g, r, and z color channels in the same image, and therefore the image contained more information about the morphology of the galaxy. The Petrosian radius of each image was used to scale the object such that the entire object fits in the image.

3. Method

Unsupervised identification of outlier images can be considered an understudied task compared to other machine vision tasks such as image classification. Unlike supervised machine learning tasks, in unsupervised machine learning the samples do not have "ground truth" labels, and therefore there is no training and test steps. Instead, the machine learning model

attempts to identify patterns in the data without associating different patterns to different labels. In the case of automatics outlier detection, a machine learning model attempts to identify the samples that are most different from the other samples in the dataset, which needs to be done without training a system based on ground truth labels. In the case of outlier galaxies, many of the galaxies of interest may be of forms that are not yet known, and therefore no training with these galaxies is possible.

Some work on outlier galaxy detection was based on adjusting deep convolutional neural networks (DCNNs) to that task. DCNNs have demonstrated superior image classification problem, but they require a relatively large number of labeled samples for training. Rare objects often do not have a large number of instances, making it more difficult to train such model. Moreover, new objects that have never been seen before do not have any existing images, making it impossible to train a CNN model. The most common approach to apply deep neural networks to automatic identification of outlier images is by using auto-encoders, where outliers can be detected by comparing the reconstruction loss of the different images (Amarbayasgalan et al., 2018; Chen et al., 2018). Such methodology was also used to identify outlier galaxies (Margapuri et al., 2020) or galaxy mergers (Margalef-Bentabol et al., 2020).

Deep neural networks provide good ability to analyze images, and are also relatively easy to implement by using commonly used deep learning libraries. On the other hand, due to their complex and non-intuitive nature, it is more difficult to control the noise that is part of almost all machine learning-based outlier detection systems. That is, when applying to datasets of millions of galaxies, even a small false positive rate of 1% could make an outlier detection algorithm impractical. That requires an algorithm that can identify outlier images, but on the other hand can also reject outlier images that are the results of known non-astronomical factors. A mandatory property of such algorithm is the ability to control the trade-off between the completeness of the algorithm, and its false-positive rate. That will allow the user to sacrifice some of the outlier galaxies that will be detected in favor of limiting the false-positive rate to make the system practical in real-world settings.

The image analysis method is based on outlier detection using machine learning and a comprehensive set of numerical image content descriptors (Shamir and Wallin, 2014; Shamir, 2021). In summary, the set of visual content descriptors include the entropy of the image, Radon transform (Lim, 1990), edge statistics, texture descriptors such as Haralick (Haralick et al., 1973), Tamura (Tamura et al., 1978) textures, and Gabor (Fogel and Sagi, 1989) textures, statistics of pixel intensities, multi-scale histograms (Hadjidemetriou et al., 2001), Zernike polynomials (Teague, 1980), fractals (Wu et al., 1992), the Gini coefficient (Abraham et al., 2003), and Chebyshev statistics. These numerical image content descriptors are described in detail in (Shamir et al., 2008, 2010, 2013; Shamir, 2016; Schutter and Shamir, 2015). The source code of the method is open and publicly available (Shamir, 2017). Previous studies have shown that the combination of these descriptors provide an effective numerical description of galaxy morphology (Shamir, 2009; Schutter and Shamir, 2015; Shamir, 2016; Shamir et al., 2013).

To select numerical image content descriptors that are informative to the detection of outlier galaxies, the content descriptors are ranked by their entropy as described by Equation 1.

$$W_f = | - 1 \cdot \Sigma_i P_i \cdot \log P_i|, \tag{1}$$

where P_i is the frequency of the values in the ith bin of a 10-bin histogram of the values of descriptor f measured from all images in the database. The W_f weight of feature f is the entropy of that feature computed by Equation 1. Low entropy of the feature reflects more consistent values, and the consistency can indicate that the values are not random, and therefore reflect the visual content.

Using the weights, the weighted distance between all pairs of images in the dataset are computed. These distance are computed by the Earth Mover's Distance (EMD). EMD is an established method for measuring distances between vectors, widely used in machine learning (Rubner et al., 2000; Ruzon and Tomasi, 2001). EMD can be conceptualized as an optimization problem, where the solution is the minimum work required to fill a set of holes in space with the mass of Earth. The unit of work is the work required to move an Earth unit by a distance unit. Equation 2 shows a formal description of the EMD optimization problem.

$$Work(X, Y, F) = \Sigma_{i=1}^{n}\Sigma_{j=1}^{n} f_{i,j} d_{i,j}, \tag{2}$$

where X and Y are the weighted feature vectors $(Wx_1, x_1).....(Wx_n, x_n)$ of size n, $f_{i,j}$ is the flow between X_i and Y_j, and W is the vector of weights. The weight vector W is computed by applying Equation 1 to all features. The flow F is the solution of the linear programming problem:

$$\Sigma_{i=1}^{n}\Sigma_{j=1}^{n} f_{i,j} = \min(\Sigma_{i=1}^{n} Wx_i, \Sigma_{j=1}^{n} Wy_j)$$

With the constraints:

$$Wx_i \geq \Sigma_{j=1}^{n} f_{i,j}$$

$$Wy_j \geq \Sigma_{i=1}^{n} f_{i,j}$$

The Earth Mover's Distance between X and Y is then defined as

$$EMD(X, Y) = \frac{Work(X,Y,F)}{\Sigma_{i=1}^{n}\Sigma_{j=1}^{n} f_{i,j}}$$

A full description of the Earth Mover's Distance method is available in (Rubner et al., 2000; Ruzon and Tomasi, 2001). The EMD method is effective for measuring distances between the histograms of all sets of numerical image content descriptors described in (Shamir et al., 2008, 2010). The distance between each pair of galaxies in the database is measured by the sum of EMD distances between all histograms.

After the similarity between each pair of images is computed, an outlier galaxy x can be detected by ranking the distances of

all galaxies from galaxy x. The N*th* shortest distance is determined to reflect the degree of difference of the galaxies from all galaxies in the database, where $N > 1$. The galaxy with the longest N*th* is determined to be the galaxy that is the most likely to be an outlier galaxy. The reason for using the N*th* shortest distance and not the shortest distance (N=1) is that in very large databases rare galaxies of the same type can appear more than once. That can lead to several galaxies similar to each other, but different from all other galaxies in the database. A short distance between the two galaxies might therefore reflect two or more outlier galaxies that are similar to each other but could be different from all other galaxies. Therefore, using the shortest distance as a measurement of how different a galaxy is from all other galaxies might lead the algorithm to a high number of false negatives.

On the other hand, some images might be different from other galaxy images in the database for certain non-astronomical reasons such as the impact of nearby very bright stars on the imaging. Examples of such images are provided in Section 4. Such artefacts make the images look very different than regular galaxies, but they are also not rare. Therefore, taking the N*th* distance can allow to avoid some of these artefacts that are common in the database. If the artefact is not common, the algorithm might falsely flag it as an outlier, increasing the false positive rate of the algorithm. In any case, the large databases of current and future astronomical sky surveys require the ability to handle the trade-off between completeness and false positive rate, as even a small false positive rate might make such algorithm impractical due to the very large number of non-outlier galaxies identified.

4. Results

The outlier detection method described in Section 3 was applied to the image data collected by the Dark Energy Survey as described in Section 2. Due to the large number of galaxies, the $2 \cdot 10^6$ galaxies were separated into 100 sets of $2 \cdot 10^4$ galaxies. Then, the algorithm described in Section 3 was applied to each of the 100 sets, returning the top 30 most peculiar images as determined by the algorithm. The value of N was set to 50. That led to a dataset of 3,000 galaxies that could be considered as possible peculiar galaxies.

As also mentioned in Section 3, the algorithm is not expected to be fully accurate in the identification of outlier galaxies. Many of the galaxies identified as outlier galaxies are not expected to indeed be of scientific interest, and therefore manual selection is required. The advantage of using the algorithm is that the manual selection is applied to 3,000 galaxies, which is several orders of magnitude less than the initial set of $2 \cdot 10^6$ DES galaxies. The 3,000 galaxies picked by the algorithms can be separated into regular galaxies, artefacts, or true positives of galaxies that could be of scientific interest.

Figure 1 shows examples of images identified by the algorithm that are different from a regular galaxy, but the difference cannot be considered of particular astronomical interest. As the figure shows, these outlier images are different from most other galaxy images, although the reasons for the differences are not necessarily of astronomical origin. The identification of artefacts and unusual images driven by non-astronomical reasons is based on previous knowledge, as these forms of outlier images are relatively common. It is therefore theoretically possible that true outlier galaxies that seem similar to common artefacts might not be identified. Figure 2 shows galaxies identified by the algorithm as outliers, although visual inspection shows that the galaxies do not have unusual features.

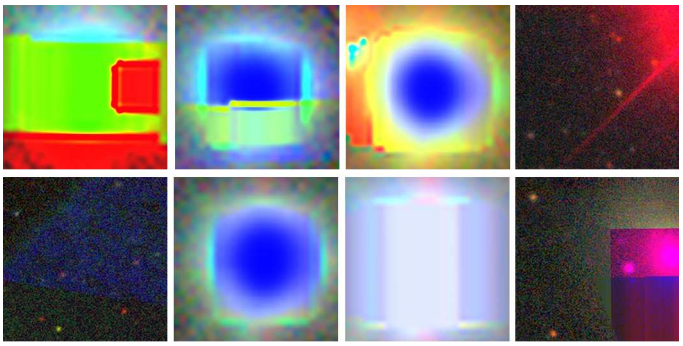

Figure 1: Objects considered galaxies that were detected by the algorithm as outliers, but visual inspection shows that these objects are not of astronomical interest.

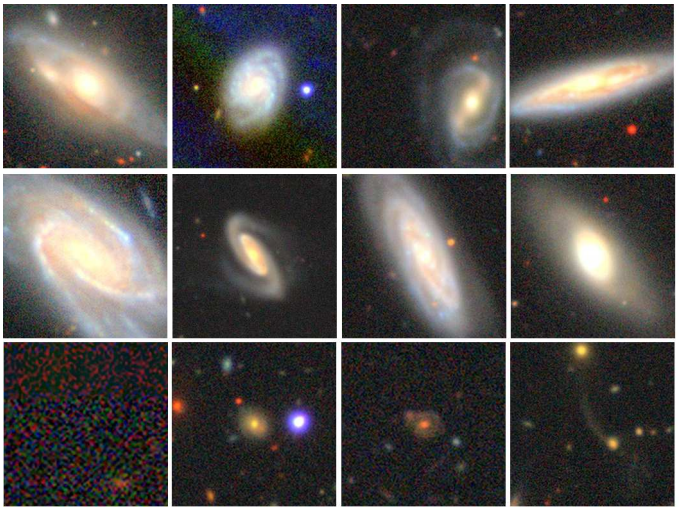

Figure 2: Galaxies that were detected by the algorithm as outliers, but seem to be regular galaxies by visual inspection.

The definition of peculiar or unusual galaxies is not necessarily formal (Nairn and Lahav, 1997), making the manual identification of all peculiar galaxies a task that is not considered of high precision. Some galaxies of scientific interest might therefore not be identified as peculiar galaxies. In this study, the selection of peculiar galaxies was done such that galaxies that belong in a known type of usual galaxies were selected based on their visual appearance. That selection was done based on previous knowledge of these galaxies, although many of the galaxies that were detected are of morphology that does not necessarily have an existing known similar instance. Like with the removal of artefact, that process of manual selection can also lead to the loss of some galaxies of scientific interest. On the

other hand, identification of peculiar galaxies when done purely by manual labor can also lead to incompleteness of the output. A notable example is the "Hanny's voorwerp" galaxy (Lintott et al., 2009), which was annotated as a regular galaxy by two more than dozens different observers, until it was identified as an unusual galaxy of scientific interest.

From the galaxies identified by the algorithm, 250 galaxies were identified by visual inspection as galaxies that could have certain features that make these galaxies different from most other galaxies. These galaxies were separated into several categories. Tables 1 through 7 show the equatorial coordinates of the galaxies detected by the algorithm, and separated into the different categories. The images of the galaxies are displayed in Figures 3 through 9.

Tables 1 and 5 list galaxies with detached segments and dust lanes. Such galaxies are not necessarily considered peculiar galaxies, but most galaxies do not have clear large detached segments or dust lanes. Object 129 is the "Cartwheel" galaxy. While that object is known, its detection shows that the algorithm can detect unusual objects automatically. Table 6 shows gravtiationally interacting systems such that the interactions change the shape of at least one of the galaxies in the system. Figure 8 displays the images of the galaxies in that table. Such galaxies are common in the Atlas of Peculiar Galaxies (Arp, 1966), but since these system are relatively rare their identification by manual inspection is a labor consuming task.

Table 2 shows possible gravitational lenses. These objects are not included in known previous catalogs of gravitational lenses such as the CASTLES survey of gravitational lenses (Kochanek et al., 1999), the catalog of SDSS gravitational lens candidates (Inada et al., 2012), gravitational lenses detected in COSMOS (Faure et al., 2008), or a survey powered by a group finding algorithm (Wilson et al., 2016). These lenses are also not present in detected gravitational lenses in HSC (Wong et al., 2018), or in catalogs compiled by using convolutional neural networks applied to DES (Jacobs et al., 2019a), or the VST Optical Imaging of the CDFS and ES1 survey (Gentile et al., 2022).

Table 7 list objects that cannot be associated clearly with any of the groups, and these galaxies are shown in Figure 9. For instance, object 252 is a galaxy with two dense arms, seemingly embedded in another, less dense, structure. The top of the system features another sparse and long arm that is not necessarily aligned with the other arms of the galaxy. Object 228 features a ring as well as a one spiral arm. Objects 232 and 244 has several rings. Object 250 also has a ring, but also has several other features making it more difficult to characterize the galaxy as a ring galaxy. Although these shapes can be the results of gravitational interaction between two or more objects, the images do not show another object that can lead to the peculiar shapes. Fully understanding each of these systems might require further detailed observation of these systems.

4.1. Performance evaluation

One of the considerations of the described algorithm is response time. The bottleneck of the analysis is the representation of each image by a set of its numerical content descriptors. Analysis of a single image required nearly two minutes using a single core of an Intel Core-i7 processor. That means that a single core can analyze the entire set of $\sim 2 \cdot 10^6$ galaxies in nearly eight years.

To handle the data, 32 cores of a Beowulf cluster were used, and reduced the response time of the system to $\sim$ 3 months of computing. While digital sky surveys are becoming increasingly more powerful, computing resources, and especially parallelizations, are also becoming more accessible. For instance, modern processors have 64 or more cores, and the availability of multiple cores in single processors is expected to grow. Therefore, while the method is computationally demanding, its requirement of computing power can be matched by the increasing availability of hardware that can be parallelized. Specifically, graphics processing units (GPUs) can be customized to parallelize the analysis, and perform a faster analysis by reducing the energy and cost of the hardware.

5. Conclusions

Autonomous digital sky surveys can acquire very large databases of astronomical data, making "traditional" manual analysis of the data impractical. Perhaps one of the more algorithmically challenging tasks is identification of peculiar astronomical object of potential interest among millions of other common astronomical objects.

This study applies a method of automatic detection of outlier galaxies imaged by the Dark Energy Survey. The experiment shows that an automated method can provide a practical solution to the problem of identification of peculiar galaxies in large databases. Although the automatic identification results in a large number of false positives, it allows to reduce the size of the data that needs to be inspected to make manual detection practical. That allows to reduce a dataset of millions of objects into a far smaller dataset of thousands of objects, of which several hundred objects are outliers.

As automatic detection of peculiar galaxies is a relatively complex task, the method shown in this paper is clearly not perfect. The advantage of the method is that it allows to control the number of alerts, and consequently handle very large image databases. The initial dataset used here of $2 \cdot 10^6$ objects was reduced to $3 \cdot 10^3$ objects, where $\sim 92\%$ of these objects were not outlier galaxies. That makes a false-positive rate of $1.375 \cdot 10^{-3}$. The true positive is obviously much lower, at $1.125 \cdot 10^{-4}$.

Digital sky surveys have been growing consistently in both power and number, and that trend in astronomy research is bound to continue. Surveys such as Vera Rubin Observatory and the space-based Euclid are further expanding the already high throughput of modern ground-based and space-based sky surveys. Due to the size of the data, it can be reasonably assumed that many objects of paramount scientific interest will be hidden in these databases, but might not be noticed. The method described here can be easily applied to data from the fourth-generation surveys and provide a large number of irregulars galaxies, peculiar galaxies, strong gravitational lenses, etc. This will significantly benefit studies of galaxy evolution and the exploration of cosmologies.

ID	RA	Dec		ID	RA	Dec		ID	RA	Dec
1	25.0160	-43.423		2	53.3290	-39.219		3	53.1833	-39.151
4	53.3321	-39.221		5	29.5303	-39.041		6	93.2225	-38.770
7	40.0661	-38.481		8	66.9333	-37.460		9	18.2232	-34.734
10	19.3597	-34.737		11	48.0650	-34.784		12	41.6079	-33.938
13	92.2672	-33.710		14	82.3580	-29.968		15	11.5389	-24.646
16	13.8953	-24.153		17	18.2169	-23.816		18	14.9967	-22.885
19	14.2179	-22.104		20	44.0267	-14.186		21	15.0158	-4.9402
22	26.1296	-4.9703		23	12.5307	-4.4804		24	10.9840	-4.2419
25	12.1810	-4.2121		26	26.3561	-3.8271		27	9.93519	-65.011
28	9.53072	-65.120		29	12.5187	-3.5511		30	15.7978	-3.6055
31	1.42831	-3.0761		32	4.27571	-2.6985		33	8.59889	-2.8351
34	1.85732	-2.3476		35	9.0261	-2.256.		36	13.0401	-2.2339
37	0.55003	-1.8722		38	3.04020	-1.8381		39	34.1008	-64.027
40	31.1652	-60.958		41	37.8805	-60.589		42	30.8068	-60.123
43	23.0091	-53.861		44	25.0463	-49.265		45	17.2175	-47.142
46	13.5656	-3.5828								

Table 1: The equatorial coordinates of detected objects with detached segments.

ID	RA	Dec		ID	RA	Dec
47	36.0262	-61.719		48	35.8424	-60.673

Table 2: The equatorial coordinates of objects detected as possible gravitational lenses.

Acknowledgment

I would like to thank the anonymous reviewer for providing comments that improved the manuscript. The research was funded by NSF grant AST-1903823.

References

Abbott, T., Abdalla, F., Allam, S., Amara, A., Annis, J., Asorey, J., Avila, S., Ballester, O., Banerji, M., Barkhouse, W., et al., 2018. The dark energy survey: data release 1. Astrophysical Journal Supplement Series 239, 18.

Abbott, T., Abdalla, F.B., Aleksić, J., Allam, S., Amara, A., Bacon, D., Balbinot, E., Banerji, M., Bechtol, K., Benoit-Lévy, A., et al., 2016. The dark energy survey: more than dark energy–an overview. Monthly Notices of the Royal Astronomical Society 460, 1270–1299.

Abraham, R.G., van den Bergh, S., 2001. The morphological evolution of galaxies. Science 293, 1273–1278.

Abraham, R.G., Van Den Bergh, S., Nair, P., 2003. A new approach to galaxy morphology. i. analysis of the sloan digital sky survey early data release. Astrophysical Journal 588, 218.

Amarbayasgalan, T., Jargalsaikhan, B., Ryu, K.H., 2018. Unsupervised novelty detection using deep autoencoders with density based clustering. Applied Sciences 8, 1468.

Appleton, P., Struck-Marcell, C., 1996. Collisional ring galaxies. Fundamentals of Cosmic Physics 16, 18.

Arp, H., 1966. Atlas of peculiar galaxies. Astrophysical Journal Supplement Series 14, 1.

Arp, H.C., Madore, B.F., 1975. A catalogue of southern peculiar galaxies from the uk schmidt survey: Preliminary reductions of 36 fields. The Observatory 95, 212–214.

Athanassoula, E., 1992. The existence and shapes of dust lanes in galactic bars. Monthly Notices of the Royal Astronomical Society 259, 345–364.

Banerji, M., Lahav, O., Lintott, C.J., Abdalla, F.B., Schawinski, K., Bamford, S.P., Andreescu, D., Murray, P., Raddick, M.J., Slosar, A., et al., 2010. Galaxy zoo: reproducing galaxy morphologies via machine learning. Monthly Notices of the Royal Astronomical Society 406, 342–353.

Bettoni, D., Galletta, G., García-Burillo, S., Rodríguez-Franco, A., 2001. The gas content of peculiar galaxies: Counterrotators and polar rings. Astronomy & Astrophysics 374, 421–434.

Buta, R.J., 2017. Galactic rings revisited–i. cvrhs classifications of 3962 ringed galaxies from the galaxy zoo 2 database. Monthly Notices of the Royal Astronomical Society 471, 4027–4046.

Casasola, V., Bettoni, D., Galletta, G., 2004. The gas content of peculiar galaxies: Strongly interacting systems. Astronomy & Astrophysics 422, 941–950.

Cecotti, H., 2020. Rotation invariant descriptors for galaxy morphological classification. International Journal of Machine Learning and Cybernetics , 1–15.

Chen, Z., Yeo, C.K., Lee, B.S., Lau, C.T., Jin, Y., 2018. Evolutionary multi-objective optimization based ensemble autoencoders for image outlier detection. Neurocomputing 309, 192–200.

Cheng, T.Y., Conselice, C.J., Aragón-Salamanca, A., Li, N., Bluck, A.F., Hartley, W.G., Annis, J., Brooks, D., Doel, P., García-Bellido, J., et al., 2020. Optimizing automatic morphological classification of galaxies with machine learning and deep learning using dark energy survey imaging. Monthly Notices of the Royal Astronomical Society 493, 4209–4228.

Conselice, C.J., 2003. The relationship between stellar light distributions of galaxies and their formation histories. Astrophysical Journal Supplement Series 147, 1.

Conselice, C.J., 2014. The evolution of galaxy structure over cosmic time. Annual Review of Astronomy and Astrophysics 52, 291–337.

Conselice, C.J., Bluck, A.F., Mortlock, A., Palamara, D., Benson, A.J., 2014. Galaxy formation as a cosmological tool–i. the galaxy merger history as a measure of cosmological parameters. Monthly Notices of the Royal Astronomical Society 444, 1125–1143.

Davis, D.R., Hayes, W.B., 2014. Sparcfire: Scalable automated detection of spiral galaxy arm segments. Astrophysical Journal 790, 87.

Diehl, T., Collaboration, D.E.S., et al., 2012. The dark energy survey camera (decam). Physics Procedia 37, 1332–1340.

Dieleman, S., Willett, K.W., Dambre, J., 2015. Rotation-invariant convolutional neural networks for galaxy morphology prediction. Monthly Notices of the Royal Astronomical Society 450, 1441–1459.

Faure, C., Kneib, J.P., Covone, G., Tasca, L., Leauthaud, A., Capak, P., Jahnke, K., Smolcic, V., De La Torre, S., Ellis, R., et al., 2008. First catalog of strong lens candidates in the cosmos field. Astrophysical Journal Supplement Series 176, 19.

Finkelman, I., Funes SJ, J.G., Brosch, N., 2012. Polar ring galaxies in the galaxy zoo. Monthly Notices of the Royal Astronomical Society 422, 2386–2398.

Flaugher, B., Diehl, H., Honscheid, K., Abbott, T., Alvarez, O., Angstadt, R.,

ID	RA	Dec		ID	RA	Dec		ID	RA	Dec
49	19.9835	-41.233		50	9.23238	-39.989		51	24.5640	-39.939
52	88.7023	-39.764		53	70.2373	-39.496		54	23.4841	-39.085
55	26.2304	-38.737		56	38.8150	-36.994		57	57.0292	-36.701
58	64.5721	-36.764		59	48.0095	-36.426		60	37.6970	-36.315
61	73.0834	-35.645		62	5.89178	-34.969		63	12.1449	-34.899
64	90.0192	-33.919		65	6.13306	-33.087		66	26.5894	-29.549
67	10.6990	-24.896		68	13.8724	-24.161		69	11.8880	-22.804
70	11.8071	-21.708		71	10.9322	-21.377		72	0.74651	-4.8807
73	13.3881	-4.6834		74	15.8261	-4.6680		75	8.24426	-65.300
76	15.5969	-4.4105		77	23.2759	-4.5320		78	10.3841	-3.8822
79	16.7885	-4.0034		80	27.8298	-4.0559		81	26.6577	-3.7783
82	2.08945	-3.6142		83	13.5512	-3.4408		84	9.21452	-2.7584
85	2.25343	-2.3795		86	1.23298	-64.769		87	7.49207	-2.3000
88	0.76150	-2.0754		89	0.84586	-1.4346		90	15.7047	-1.4702
91	12.1583	-64.520		92	12.8725	-64.356		93	16.8820	-64.233
94	23.6451	-64.353		95	14.1570	0.10382		96	25.8844	-63.967
97	18.2076	0.98033		98	8.25643	-62.567		99	12.5641	-59.892
100	12.8893	-59.708		101	12.8893	-59.080		102	16.3372	-57.229
103	86.6126	-53.999		104	18.3707	-52.304		105	10.1921	-51.463

Table 3: The coordinates of detected irregular blue galaxies.

Annis, J., Antonik, M., Ballester, O., Beaufore, L., et al., 2015. The dark energy camera. Astronomical Journal 150, 150.

Fogel, I., Sagi, D., 1989. Gabor filters as texture discriminator. Biological Cybernetics 61, 103–113.

Gallagher, J.S., Hunter, D.A., 1984. Structure and evolution of irregular galaxies. Annual Review of Astronomy and Astrophysics 22, 37–74.

Gentile, F., Tortora, C., Covone, G., Koopmans, L.V., Spiniello, C., Fan, Z., Li, R., Liu, D., Napolitano, N.R., Vaccari, M., et al., 2022. Lenses in voice (live): searching for strong gravitational lenses in the voice@ vst survey using convolutional neural networks. Monthly Notices of the Royal Astronomical Society 510, 500–514.

Gillman, S., Tiley, A., Swinbank, A., Harrison, C., Smail, I., Dudzevičiūtė, U., Sharples, R., Cortese, L., Obreschkow, D., Bower, R., et al., 2020. From peculiar morphologies to hubble-type spirals: the relation between galaxy dynamics and morphology in star-forming galaxies at z 1.5. Monthly Notices of the Royal Astronomical Society 492, 1492–1512.

Goddard, H., Shamir, L., 2020. A catalog of broad morphology of pan-starrs galaxies based on deep learning. Astrophysical Journal Supplement Series 251, 28.

Graham, A.W., 2019. A galaxy classification grid that better recognizes early-type galaxy morphology. Monthly Notices of the Royal Astronomical Society 487, 4995–5009.

Hadjidemetriou, E., Grossberg, M.D., Nayar, S.K., 2001. Spatial information in multiresolution histograms, in: Proceedings of the IEEE Computer Society Conference on Computer Vision and Pattern Recognition, IEEE. pp. I–I.

Haralick, R.M., Shanmugam, K., Dinstein, I.H., 1973. Textural features for image classification. IEEE Transactions on Systems, Man, and Cybernetics , 610–621.

Hosny, K., Elaziz, M., Selim, I., Darwish, M., 2020. Classification of galaxy color images using quaternion polar complex exponential transform and binary stochastic fractal search. Astronomy and Computing , 100383.

Huang, X., Storfer, C., Ravi, V., Pilon, A., Domingo, M., Schlegel, D., Bailey, S., Dey, A., Gupta, R., Herrera, D., et al., 2020. Finding strong gravitational lenses in the desi decam legacy survey. Astrophysical Journal 894, 78.

Huertas-Company, M., Gravet, R., Cabrera-Vives, G., Pérez-González, P., Kartaltepe, J., Barro, G., Bernardi, M., Mei, S., Shankar, F., Dimauro, P., et al., 2015a. A catalog of visual-like morphologies in the 5 candels fields using deep-learning. arXiv preprint arXiv:1509.05429 .

Huertas-Company, M., Pérez-González, P.G., Mei, S., Shankar, F., Bernardi, M., Daddi, E., Barro, G., Cabrera-Vives, G., Cattaneo, A., Dimauro, P., et al., 2015b. The morphologies of massive galaxies from z˜ 3-witnessing the 2 channels of bulge growth. arXiv preprint arXiv:1506.03084 .

Huertas-Company, M., Tasca, L., Rouan, D., Pelat, D., Kneib, J., Le Fevre, O., Capak, P., Kartaltepe, J., Koekemoer, A., Mccracken, H., et al., 2009. A robust morphological classification of high-redshift galaxies using support vector machines on seeing limited images. Astronomy and Astrophysics 497, 743.

Inada, N., Oguri, M., Shin, M.S., Kayo, I., Strauss, M.A., Morokuma, T., Rusu, C.E., Fukugita, M., Kochanek, C.S., Richards, G.T., et al., 2012. The sloan digital sky survey quasar lens search. v. final catalog from the seventh data release. Astronomical Journal 143, 119.

Jacobs, C., Collett, T., Glazebrook, K., Buckley-Geer, E., Diehl, H., Lin, H., McCarthy, C., Qin, A., Odden, C., Escudero, M.C., et al., 2019a. An extended catalog of galaxy–galaxy strong gravitational lenses discovered in des using convolutional neural networks. Astrophysical Journal Supplement Series 243, 17.

Jacobs, C., Collett, T., Glazebrook, K., McCarthy, C., Qin, A., Abbott, T., Abdalla, F., Annis, J., Avila, S., Bechtol, K., et al., 2019b. Finding high-redshift strong lenses in des using convolutional neural networks. Monthly Notices of the Royal Astronomical Society 484, 5330–5349.

Kaviraj, S., 2010. Peculiar early-type galaxies in the sloan digital sky survey stripe82. Monthly Notices of the Royal Astronomical Society 406, 382–394.

Kochanek, C., Falco, E., Impey, C., Lehár, J., McLeod, B., Rix, H.W., 1999. Results from the castles survey of gravitational lenses, in: AIP Conference Proceedings, American Institute of Physics. pp. 163–175.

Kuminski, E., George, J., Wallin, J., Shamir, L., 2014. Combining human and machine learning for morphological analysis of galaxy images. Publications of the Astronomical Society of the Pacific 126, 959–967.

Kuminski, E., Shamir, L., 2016. A computer-generated visual morphology catalog of 3,000,000 sdss galaxies. Astrophysical Journal Supplement Series 223, 20.

Lim, J.S., 1990. Two-dimensional signal and image processing. New Haven: Prentice Hall .

Lintott, C.J., Schawinski, K., Keel, W., Van Arkel, H., Bennert, N., Edmondson, E., Thomas, D., Smith, D.J., Herbert, P.D., Jarvis, M.J., et al., 2009. Galaxy zoo:'hanny's voorwerp', a quasar light echo? Monthly Notices of the Royal Astronomical Society 399, 129–140.

Liu, C., Zhang, Z., Li, J., Li, Y., Zou, Z., 2021. Recognition of astronomical strong gravitational lens system based on deep learning, in: 2021 9th International Conference on Intelligent Computing and Wireless Optical Communications (ICWOC), IEEE. pp. 58–63.

Madore, B.F., Nelson, E., Petrillo, K., 2009. Atlas and catalog of collisional ring galaxies. Astrophysical Journal Supplement Series 181, 572.

Margalef-Bentabol, B., Huertas-Company, M., Charnock, T., Margalef-

ID	RA	Dec		ID	RA	Dec		ID	RA	Dec
106	21.8298	-44.064		107	14.2471	-43.842		108	316.708	-40.356
109	22.3453	-39.905		110	29.5910	-39.879		111	20.3687	-39.677
112	21.8018	-39.836		113	22.1732	-39.637		114	24.1116	-39.413
115	29.4474	-39.440		116	22.1516	-39.307		117	18.0015	-38.913
118	21.4559	-39.105		119	21.9585	-39.030		120	43.6317	-39.067
121	75.2043	-38.876		122	24.6654	-38.764		123	80.6596	-37.752
124	88.6841	-36.522		125	31.7459	-35.719		126	44.6345	-34.677
127	20.9356	-34.461		128	41.7983	-34.427		129	9.43734	-33.705
130	18.7599	-32.234		131	18.0802	-32.061		132	20.2459	-29.211
133	10.4466	-24.387		134	12.7404	-23.557		135	10.3802	-22.641
136	15.3996	-22.059		137	48.4839	-14.969		138	25.6132	-14.533
139	20.3018	-14.243		140	20.3157	-13.793		141	23.3719	-13.863
142	6.83340	-4.8914		143	10.3298	-4.9730		144	12.3963	-4.9378
145	14.4237	-4.9554		146	16.1468	-4.6820		147	29.1036	-4.4724
148	6.31877	-2.7616		149	28.2879	-64.772		150	34.7829	-64.804
151	9.02329	-2.3321		152	9.51328	-2.3177		153	1.38100	-2.1122
154	0.04351	-1.5109		155	27.4904	-64.487		156	23.7545	-64.243
157	26.0110	-64.370		158	18.3670	0.14845		159	14.0249	0.62863
160	26.7319	-64.019		161	9.87239	-63.768		162	11.2942	-63.728
163	36.1261	-61.662		164	32.1129	-60.141		165	233.126	52.6243
166	230.236	54.6749		167	57.6141	-54.149		168	24.4276	-53.779
169	19.8673	-51.772		170	24.7202	-49.785		171	26.0838	-49.760
172	23.2804	-49.199		173	22.6231	-48.838		174	357.852	10.8401
175	13.0401	-2.2339		176	358.825	11.2425		177	359.842	10.6572

Table 4: The coordinates of detected possible ring galaxies.

ID	RA	Dec		ID	RA	Dec		ID	RA	Dec
178	28.5414	-44.033		179	20.7624	-43.127		180	18.0030	-33.564
181	19.9193	-33.100		182	13.5783	-23.554		183	17.9328	-23.305
184	18.9117	-23.255		185	20.1795	-14.732		186	28.5135	-14.253
187	41.2831	-13.236		188	27.6655	-3.9382		189	13.5655	-3.5895
190	18.2573	-64.826		191	13.9032	-63.736		192	29.5756	-54.215
193	14.0309	-53.189		194	14.2397	-52.923				

Table 5: The coordinates of detected possible galaxies with dust lanes.

Bentabol, C., Bernardi, M., Dubois, Y., Storey-Fisher, K., Zanis, L., 2020. Detecting outliers in astronomical images with deepgenerative networks. arXiv:2003.08263 .

Margapuri, V.S.K., Shamir, L., Thapa, B., 2020. Detection of unknown galaxy types in large databases of galaxy images, in: 29th International Conference on Software Engineering and Data Engineering, ISCA.

Mittal, A., Soorya, A., Nagrath, P., Hemanth, D.J., 2019. Data augmentation based morphological classification of galaxies using deep convolutional neural network. Earth Science Informatics , 1–17.

Möllenhoff, C., Bender, R., 1989. The peculiar kinematics of the elliptical dust-lane galaxy ngc 4589. Astronomy and Astrophysics 214, 61–67.

Morganson, E., Gruendl, R., Menanteau, F., Kind, M.C., Chen, Y.C., Daues, G., Drlica-Wagner, A., Friedel, D., Gower, M., Johnson, M., et al., 2018. The dark energy survey image processing pipeline. Publications of the Astronomical Society of the Pacific 130, 074501.

Nair, P.B., Abraham, R.G., 2010. A catalog of detailed visual morphological classifications for 14,034 galaxies in the sloan digital sky survey. Astrophysical Journal Supplement Series 186, 427.

Nairn, A., Lahav, O., 1997. What is a peculiar galaxy? Monthly Notices of the Royal Astronomical Society 286, 969–978.

Peng, C.Y., Ho, L.C., Impey, C.D., Rix, H.W., 2002. Detailed structural decomposition of galaxy images. Astronomical Journal 124, 266.

Perez, S.J.A., Nichol, B., Percival, W., Thomas, D.B., Collaboration, D., et al., 2018. The dark energy survey: Data release 1. Astrophysical Journal Supplement Series 239, 18.

Petrillo, C., Tortora, C., Chatterjee, S., Vernardos, G., Koopmans, L., Verdoes Kleijn, G., Napolitano, N.R., Covone, G., Kelvin, L., Hopkins, A.M., 2019. Testing convolutional neural networks for finding strong gravitational lenses in kids. Monthly Notices of the Royal Astronomical Society 482, 807–820.

Rubner, Y., Tomasi, C., Guibas, L.J., 2000. The earth mover's distance as a metric for image retrieval. International Journal of Computer Vision 40, 99–121.

Ruzon, M.A., Tomasi, C., 2001. Edge, junction, and corner detection using color distributions. IEEE Transactions on Pattern Analysis and Machine Intelligence 23, 1281–1295.

Schutter, A., Shamir, L., 2015. Galaxy morphology—an unsupervised machine learning approach. Astronomy and Computing 12, 60–66.

Sellwood, J., Moore, E., 1999. On the formation of disk galaxies and massive central objects. Astrophysical Journal 510, 125.

Shamir, L., 2009. Automatic morphological classification of galaxy images. Monthly Notices of the Royal Astronomical Society 399, 1367–1372.

Shamir, L., 2011. Ganalyzer: A tool for automatic galaxy image analysis. Astrophysical Journal 736, 141.

Shamir, L., 2016. Morphology-based query for galaxy image databases. Publications of the Astronomical Society of the Pacific 129, 024003.

ID	RA	Dec		ID	RA	Dec		ID	RA	Dec
195	25.0351	-43.740		196	46.5785	-39.344		197	71.0259	-38.484
198	66.6586	-36.038		199	91.7963	-35.067		200	19.9831	-34.265
201	11.0489	-24.322		202	10.7240	-23.545		203	13.9377	-23.478
204	42.8310	-13.355		205	1.49017	-4.9928		206	0.18903	-4.7813
207	7.08776	-4.8255		208	14.8486	-4.8032		209	11.2310	-4.1358
210	1.02484	-4.0871		211	24.3611	-64.896		212	15.9150	-2.3332
213	1.37269	-2.0939		214	0.32218	-1.5197		215	11.4851	-63.729
216	16.1720	-63.829		217	33.0961	-60.101		218	230.280	50.6720
219	26.1203	-49.790		220	22.4344	-48.891		221	13.2715	-2.4701
222	358.047	11.4678								

Table 6: The coordinates of detected objects that can be tidally distorted systems.

ID	RA	Dec		ID	RA	Dec		ID	RA	Dec
223	14.2833	-43.727		224	23.8920	-43.410		225	54.8327	-38.975
226	77.3550	-38.464		227	6.01508	-34.960		228	12.9062	-34.886
229	23.4023	-29.885		230	23.7417	-29.759		231	22.3487	-28.631
232	11.7824	-24.376		233	10.7661	-22.247		234	10.7245	-22.257
235	25.2616	-14.314		236	23.2281	-13.864		237	42.8663	-13.298
238	28.5265	-4.8778		239	5.04152	-4.4164		240	11.0260	-4.4902
241	17.8263	-4.0600		242	22.3028	-3.8874		243	11.9790	-3.5191
244	12.1786	-64.994		245	5.06276	-2.6528		246	4.75718	-2.4539
247	16.0499	-2.0576		248	7.40026	-1.7385		249	122.447	5.01916
250	33.2834	-61.752		251	36.5613	-61.631		252	30.8603	-61.218

Table 7: The coordinates of other galaxies identified as outlier galaxies.

Shamir, L., 2017. Udat: A multi-purpose data analysis tool. Astrophysics Source Code Library , ascl:1704.002.

Shamir, L., 2020. Automatic detection of full ring galaxy candidates in sdss. Monthly Notices of the Royal Astronomical Society 491, 3767–3777.

Shamir, L., 2021. Automatic identification of outliers in hubble space telescope galaxy images. Monthly Notices of the Royal Astronomical Society 501, 5229–5238.

Shamir, L., Holincheck, A., Wallin, J., 2013. Automatic quantitative morphological analysis of interacting galaxies. Astronomy and Computing 2, 67–73.

Shamir, L., Macura, T., Orlov, N., Eckley, D.M., Goldberg, I.G., 2010. Impressionism, expressionism, surrealism: Automated recognition of painters and schools of art. ACM Transactions on Applied Perception 7, 1–17.

Shamir, L., Orlov, N., Eckley, D.M., Macura, T., Johnston, J., Goldberg, I.G., 2008. Wndchrm–an open source utility for biological image analysis. Source Code for Biology and Medicine 3, 13.

Shamir, L., Wallin, J., 2014. Automatic detection and quantitative assessment of peculiar galaxy pairs in sloan digital sky survey. Monthly Notices of the Royal Astronomical Society 443, 3528–3537.

Simard, L., 1999. Photometric redshifts and the luminosity-size relation of galaxies to z= 1. 1, in: Photometric Redshifts and the Detection of High Redshift Galaxies, p. 325.

Suyu, S.H., Bonvin, V., Courbin, F., Fassnacht, C.D., Rusu, C.E., Sluse, D., Treu, T., Wong, K., Auger, M.W., Ding, X., et al., 2017. H0licow–i. h0 lenses in cosmograil's wellspring: program overview. Monthly Notices of the Royal Astronomical Society 468, 2590–2604.

Tamura, H., Mori, S., Yamawaki, T., 1978. Textural features corresponding to visual perception. IEEE Transactions on Systems, Man, and Cybernetics 8, 460–473.

Taylor, V.A., Jansen, R.A., Windhorst, R.A., Odewahn, S.C., Hibbard, J.E., 2005. Ubvr and hubble space telescope mid-ultraviolet and near-infrared surface photometry and radial color gradients of late-type, irregular, and peculiar galaxies. Astrophysical Journal 630, 784.

Teague, M.R., 1980. Image analysis via the general theory of moments. Journal of the Optical Society of America 70, 920–930.

Timmis, I., Shamir, L., 2017. A catalog of automatically detected ring galaxy candidates in panstarss. Astrophysical Journal Supplement Series 231, 2.

Wilde, J., Serjeant, S., Bromley, J.M., Dickinson, H., Koopmans, L.V., Metcalf, R.B., 2022. Detecting gravitational lenses using machine learning: exploring interpretability and sensitivity to rare lensing configurations. Monthly Notices of the Royal Astronomical Society 512, 3464–3479.

Wilson, M.L., Zabludoff, A.I., Ammons, S.M., Momcheva, I.G., Williams, K.A., Keeton, C.R., 2016. A spectroscopic survey of the fields of 28 strong gravitational lenses: The group catalog. Astrophysical Journal 833, 194.

Wong, K.C., Chan, J.H., Chao, D.C., Jaelani, A.T., Kayo, I., Lee, C.H., More, A., Oguri, M., 2022. Survey of gravitationally lensed objects in hsc imaging (sugohi). viii. new galaxy-scale lenses from the hsc ssp. Publications of the Astronomical Society of Japan 74, 1209–1219.

Wong, K.C., Sonnenfeld, A., Chan, J.H., Rusu, C.E., Tanaka, M., Jaelani, A.T., Lee, C.H., More, A., Oguri, M., Suyu, S.H., et al., 2018. Survey of gravitationally lensed objects in hsc imaging (sugohi). ii. environments and line-of-sight structure of strong gravitational lens galaxies to z 0.8. Astrophysical Journal 867, 107.

Wong, K.C., Suyu, S.H., Chen, G.C., Rusu, C.E., Millon, M., Sluse, D., Bonvin, V., Fassnacht, C.D., Taubenberger, S., Auger, M.W., et al., 2020. H0licow–xiii. a 2.4 per cent measurement of h 0 from lensed quasars: 5.3 σ tension between early-and late-universe probes. Monthly Notices of the Royal Astronomical Society 498, 1420–1439.

Wu, C.M., Chen, Y.C., Hsieh, K.S., 1992. Texture features for classification of ultrasonic liver images. IEEE Transactions on Medical Imaging 11, 141–152.

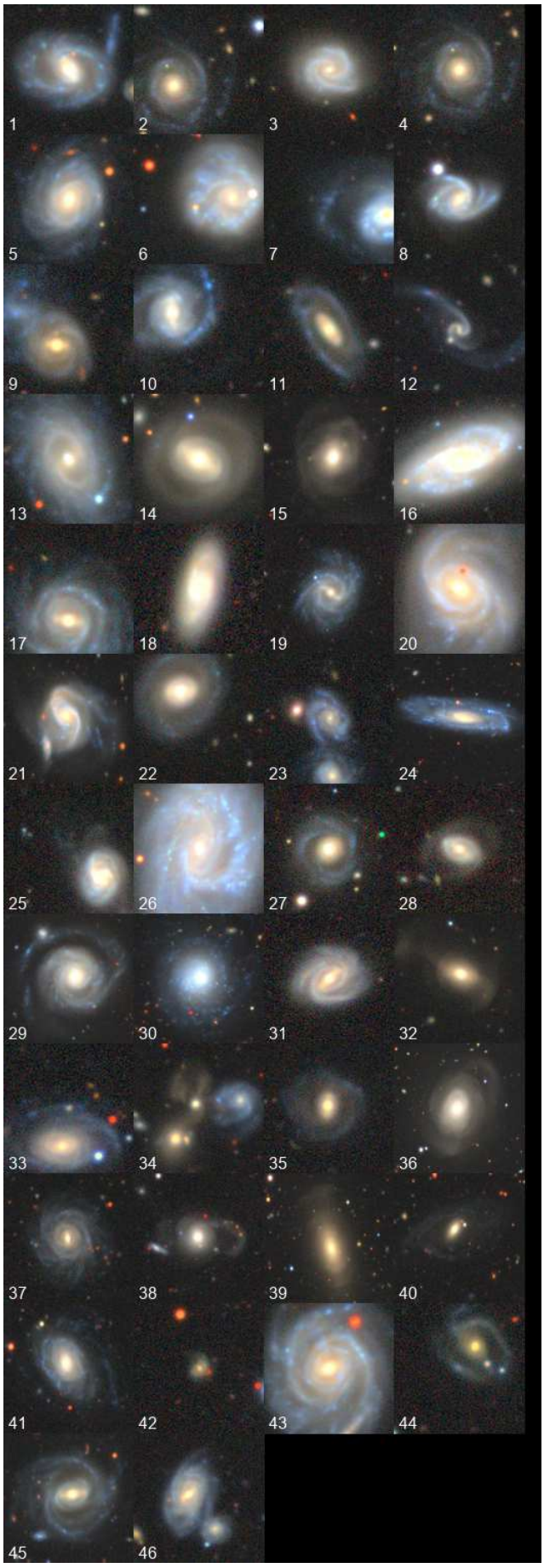

Figure 3: Galaxies with detached segments that were detected by the algorithm.

Figure 4: Galaxies that are possible gravitational lenses.

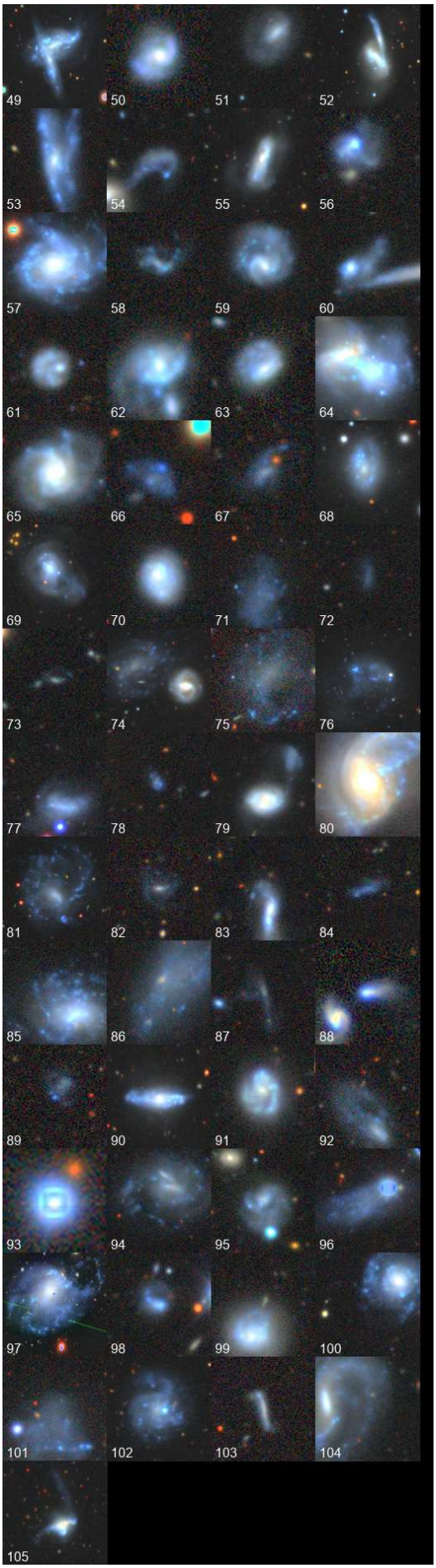

Figure 5: Irregular blue galaxies detected in DES.

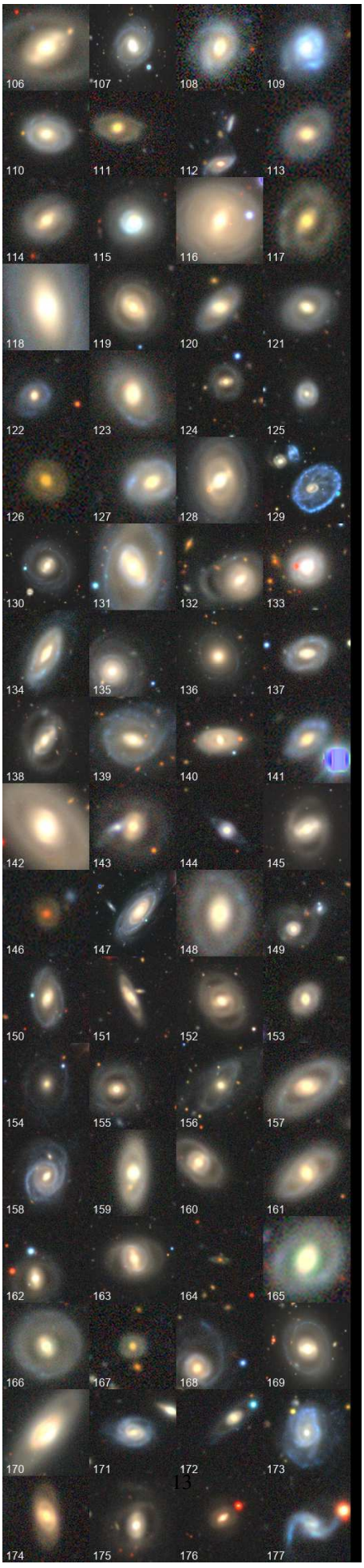

Figure 6: Ring galaxies detected in DES.

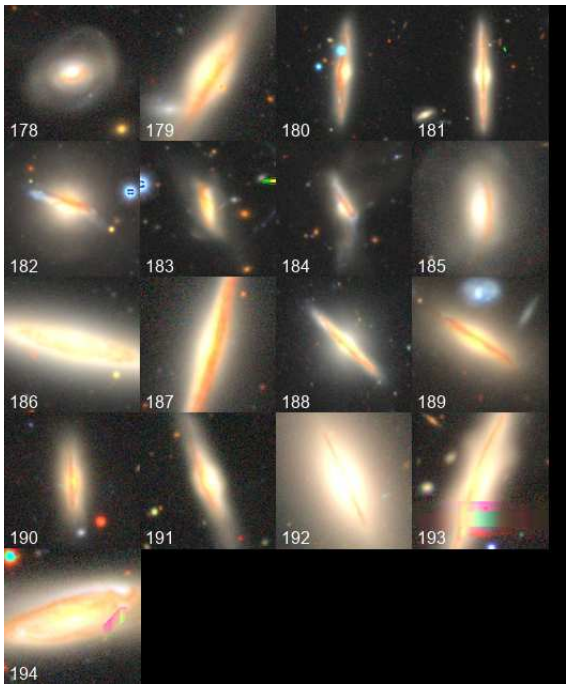

Figure 7: Galaxies with dust lanes.

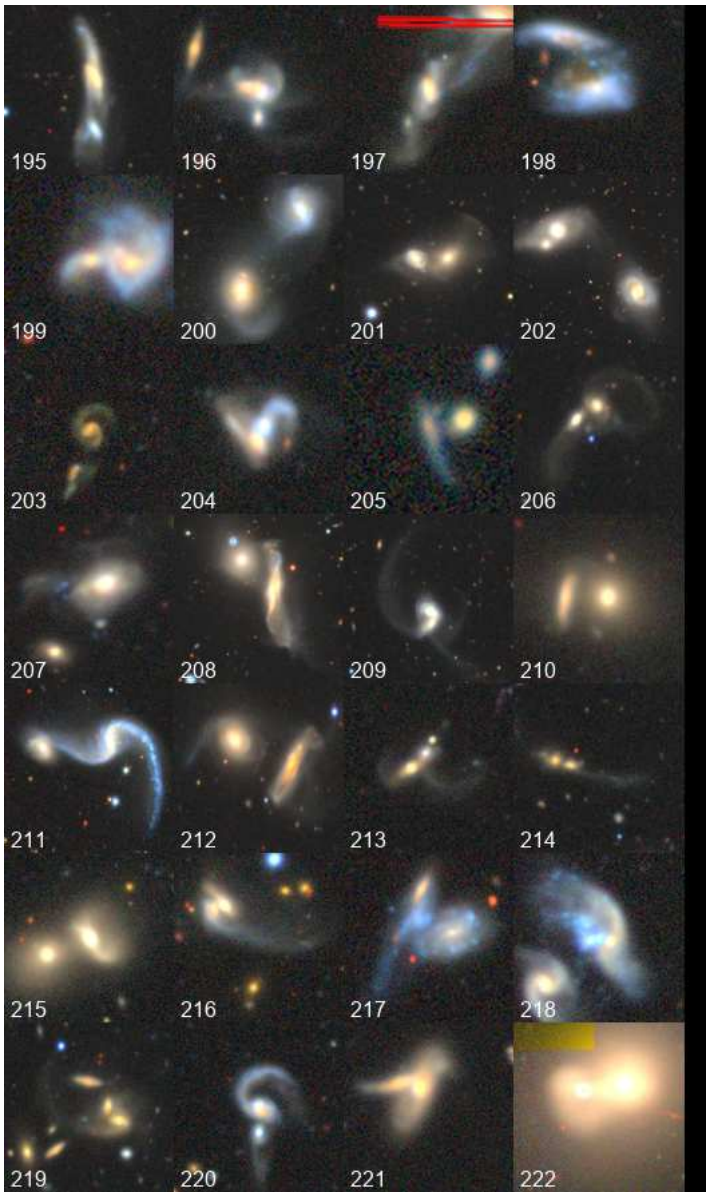

Figure 8: Images of detected objects that can be tidally distorted systems.

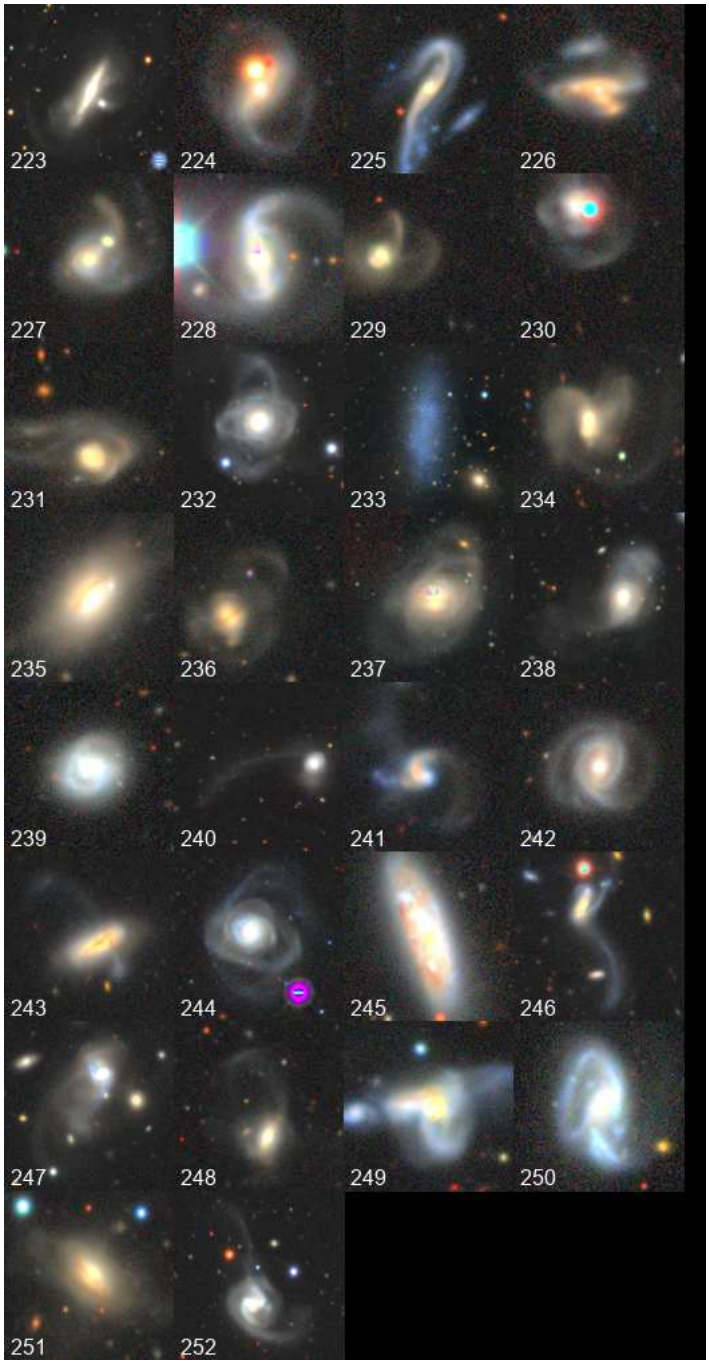

Figure 9: Unusual galaxies that are not associated to the previous categories.